scientific reports

OPEN

Exploration of selenophene analogue and different acceptor influence on photovoltaic properties of pyrrole-4,6(5-*H*)-dione based chromophores via quantum chemical investigations

Muhammad Khalid[1,2]✉, Fatima Tayyab[1,2], Muhammad Adeel[1,2], Nayab Tahir[3], Ataualpa A. C. Braga[4] & Khalid Abdullah Alrashidi[5]

Non-fullerene organic compounds are considered efficient photovoltaic materials in the development of solar cells. Therefore, considering the importance of non-fullerene organic compounds, a series of non-fullerene organic chromophores (SPF1–SPF6) was designed via molecular engineering at terminal acceptors of reference compound (SPFR). Further, owing to the interesting features of selenium than sulphur towards charge transfer, thiophene was replaced with selenophene in designed derivatives and analyzed using quantum chemical approach. Through benchmark study, CAM-B3LYP/6-311G(d, p) functional was selected for the current study. Several parameters, such as frontier molecular orbitals, density of states, binding energy, transition density matrix, optical properties, reorganization energies of electron and hole, open circuit voltage, and charge transfer analyses were assessed to comprehend the photovoltaic properties of designed compounds. A energy gap: 4.433–4.764 eV with absorption spectra as 465.1–512.7 nm in chloroform and 445.4–494.0 nm in the gas phase and greater charge transference rate was studied in selenophene derivatives. The lower E_b and the behavior of holes and electrons implied a higher rate of exciton separation and considerable transfer of charges towards LUMO from the HOMO. The results of DOS and TDM analysis further corroborated these findings. Furthermore, the V_{oc}, in relation to the $\text{HOMO}_{\text{PTB7}}$–$\text{LUMO}_{\text{Acceptor}}$, depicted that the proposed molecules have good V_{oc} values. Furthermore, a comparative study with spiro-OMeTAD, a standard hole transport material (HTM) demonstrated a good correlation, indicating that the proposed compounds have the potential to function as efficient HTMs. Therefore, it can be deduced that the use of molecular engineering with various acceptor molecules has the potential to enhance the effectiveness of photovoltaic materials.

Keywords Selenophene, Molecular engineering, DFT, Photovoltaic response, Acceptor modifications, Fullerene free chromophores

Scientists are currently investigating renewable energy sources, including wind, water, biomass, and particularly solar cells, because of their limitless and eco-friendly nature[1]. Solar energy, with an enormous energy output of 3.8×10^{33} ergs per second, is harnessed by solar cells through the photovoltaic effect, where photons create electron–hole pairs in semiconductors, ultimately generating electricity[2]. Historically, photovoltaic systems using

[1]Institute of Chemistry, Khwaja Fareed University of Engineering & Information Technology, Rahim Yar Khan 64200, Pakistan. [2]Centre for Theoretical and Computational Research, Khwaja Fareed University of Engineering & Information Technology, Rahim Yar Khan 64200, Pakistan. [3]Wellman Center for Photomedicines, Massachusetts General Hospital, Harvard Medical School, Boston, MA 02114, USA. [4]Department of Fundamental Chemistry, Institute of Chemistry, University of Sao Paulo, Av. Prof. Lineu Prestes, 748, Sao Paulo 05508-000, Brazil. [5]Department of Chemistry, College of Science, King Saud University, P.O. Box 2455, Riyadh 11451, Saudi Arabia. ✉email: muhammad.khalid@kfueit.edu.pk

silicon as the primary material have been recognized for their affordability and robustness. Silicon is extensively used in photovoltaic silicon-based energy devices because of its notable efficiency, durability, cost-effectiveness, abundance, and environmentally benign characteristics[3]. However, it has been noticed in recent times that silicon is costly, delicate, and cannot adjust its energy levels[4]. In addition, the organic bulk heterojunction solar cells (BHJ) have been identified as potential alternatives[5]. The manufacturing of flexible large-area devices is associated with several benefits that contribute to their prevalence. Additionally, these devices are more cost-effective compared to alternative options that rely on inorganic materials[6,7]. Hence, there is significant research being conducted on fullerene-based solar cells owing to their significant photovoltaic characteristics[8]. Nevertheless, several drawbacks have emerged about this material. These include the high cost associated with the manufacturing process, decreased efficiency in capturing sunlight, inability to adjust the LUMO energy, and a lack of reliability in terms of structure[9]. The presence of these anomalies renders fullerene acceptors less effective materials. Consequently, the researchers shifted their focus towards non-fullerene acceptors (NFAs) owing to their suitable energy levels, modifiable architectures, wide absorption spectra, and cost-effectiveness. To optimize the photovoltaic characteristics of recently developed compounds used in non-fullerene OSCs, the most effective approach is to reduce the energy difference between their HOMOs and LUMOs. This is achieved by taking into account their structure-property relationship, such as effective electron-donating and electron-withdrawing components[10].

Small molecules that have an A–π–A–π–A structure, consisting of two electron-withdrawing units at the ends, two π-bridges connecting the acceptor units to a central core electron-donating unit, exhibit superior photovoltaic performance compared to other small molecules of the donor-acceptor (D-A) type[11,12]. NFAs have intriguing optical absorption properties, with their absorbance extending into the infrared (IR) region. The power conversion efficiency (PCE) of organic photovoltaics (OPVs) is improved by greater molar absorption coefficients of NFAs. The implementation of end-capped modifications is regarded as a very effective approach for enhancing the optoelectronic characteristics of materials used in solar applications[13]. This method allows precise energy level adjustment while minimally impacting molecular stacking. Halogen-containing NFAs exhibit enhanced crystallinity, charge carrier mobility, and molecular planarity due to non-covalent intermolecular interactions. Consequently, many newly designed compounds incorporate –Cl, –F, and –CN groups as terminal electron-withdrawing moieties to improve the optoelectronic properties and ICT[14].

Pyrrole-4,6(5 H)-dione-based chromophores have recently emerged as promising candidates for photovoltic materials due to their strong electron-accepting nature, excellent charge transport properties, and tunable optoelectronic characteristics[15]. Their unique molecular structure allows for efficient hole mobility and favorable energy level alignment with perovskite layers, ensuring effective charge extraction and transport[16]. Furthermore, these compounds offer structural versatility, enabling fine-tuning of their electronic properties through end-cap and core modifications. Compared to conventional HTMs, pyrrole-4,6(5 H)-dione derivatives provide enhanced stability and processability, making them attractive for scalable photovoltaic applications[17].

The selenophene derivatives are much more promising in the development of light-sensitive materials for photovoltaic applications. Selenium exhibits greater polarizability compared to sulfur due to its larger and more loosely distributed outermost electron cloud[18]. This characteristic enhances the interactions between selenium atoms (Se–Se) in solid-state materials and contributes to higher charge carrier mobility in such materials[19]. To further enhance their efficiency, it would be advantageous to generate additional absorption bands within the visible light spectrum.

This paper employs the modification of parent molecule (TPD-T-CN)[20], which is abbreviated as SPFR in this article, by replacing its thiophene with selenophene rings (SPF1), which act as π -spacer. Furthermore, six new molecules with A_1–π–A_2–π–A_1 structure are designed, each with distinct terminal end-capped acceptor units. The involvement of the selenophene bridges in prolonging the conjugation is significant as it aids in facilitating the charge transfer (CT) from the core toward terminals. Moreover, this study provides a comprehensive analysis of various factors such as frontier molecular orbital analysis, transition matrix density, excitation energy, binding energy, open circuit voltage, reorganizational energy, and hole-electron analysis. These analyses are conducted on a set of designed molecules (SPF1–SPF6), which are compared with SPFR. This investigation aims to evaluate the potential of these novel NFAs regarding their optoelectronic characteristics and their use in next-generation solar cells.

Computational procedure

The current study examines the geometrical, optical, electronic, and photovoltaic characteristics of the selenophene-based compounds via DFT/TD-DFT approaches. CAM-B3LYP functional was selected through benchmark study between the experimental reported value of SPFR (477 nm)[20] and its simulated values calculated at different sophisticated functional. At first, four different functionals: B3LYP[21], MPW1PW91[22], M06[23], and CAM-B3LYP[24] with 6-311 g(d, p)[25] basis set were employed to optimize the SPFR. The calculations were performed with the Gaussian 09 software[26], while the visualization of the obtained findings was facilitated using GaussView 5.0[27] program. The absorption maximum of SPFR was calculated on above-mentioned functionals using TD-DFT. The simulated λ_{max} of SPFR at above mentioned functionals were found to be 540.920, 513.976, 514.223, and 442.611 nm, respectively. The experimental λ_{max} of SPFR was reported to be 477 nm[20]. The outcome of λ_{max} calculation indicates that the CAM-B3LYP/6–311 g(d, p) method exhibited the concordance with the experimental λ_{max} value (Fig. 1), therefore, this functional was selected for further computational analyses of titled compounds. The optimization energy of entitled compounds is illustrated in Fig. S9. Furthermore, the above-mentioned functional was used to investigate other properties like DOS, FMOs, UV-Vis, TDM, V_{oc}, E_b, and hole-electron analyses. Various software such as PyMOlyze version 2.0[28], Multiwfn version 3.7[29], GaussView version 5.0[27], Avogadro version 1.2.0n[30], and Chemcraft[31] were employed for data interpretation.

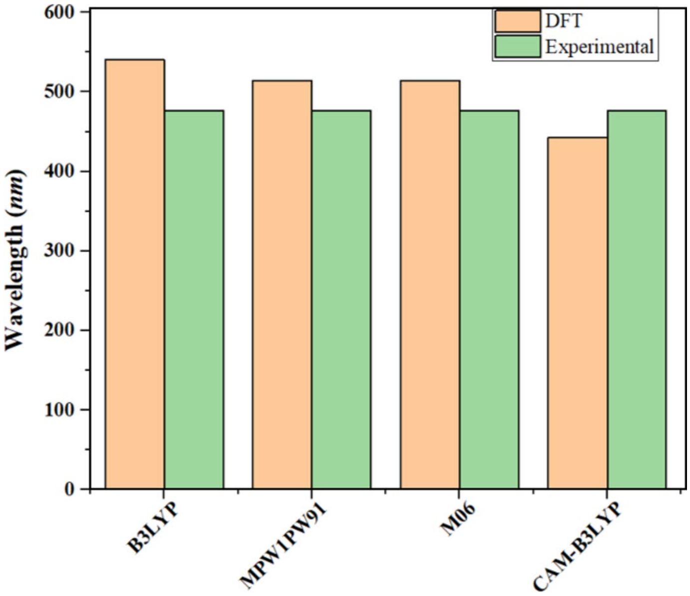

Fig. 1. Comparison between simulated and experimental UV–Vis data of SPFR at different functional.

Results and discussion

Melanie et al. synthesized NF-based small molecule (TPD-T-CN) by robust stille coupling reaction. TPD-T-CN has $A_2-\pi-A_1-\pi-A_2$ configuration in which thiophene rings act as π -spacers while the dicyanovinyl (–CN) is used as terminal acceptor. In the current work, SPFR is used as reference compound to design six new derivatives. In SPF1, thiophene rings are replaced with selenophene, which is then acting as linker. Furthermore, five new 5-methyl-4-*H*-selenopheno[3,4-c]pyrrole-4,6(5-*H*)-dione core-based acceptor molecules (SPF2–SPF6) have been designed *via* the structural tailoring approach with efficient acceptors. The end-capped acceptor modifications of SPF1 is done with 2-(2-methylene-3-oxo-2,3-dihydro-1-*H*-inden-1-ylidene)malononitrile (SPF2), (2-methylene-3-oxo-2,3-dihydro-1-*H*-inden-1-ylidene)methylene dinitrate (SPF3), (2,3-dimethylene-2,3-dihydro-1-*H*-inden-1-ylidene)methanedisulfonic acid (SPF4), 2-methylene-3-(perfluoropropan-2-ylidene)-2,3-dihydro-1-*H*-inden-1-one (SPF5), and dimethyl 2-(2-methylene-3-oxo-2,3-dihydro-1-*H*-inden-1-ylidene) malonate (SPF6)[32,33] acceptors as shown in Fig. 2a. The selenophene rings act as the π –spacer in all designed derivatives (Fig. S1). The optimized structures of these chromophores are presented in Fig. 2b and Tables S1–S7 include cartesian coordinates. Literature indicates that a reaction with a negative ΔG° value signifies spontaneity and substantial product production[34]. The negative ΔG° values for the examined compounds are derived from equation S1, as seen in Table S25, which demonstrates the possibility of product production (SPFR and SPF1–SPF6) and their stability. Moreover, the computed geometrical parameters, i.e., bond lengths (Å) and bond angles (°), are presented in Tables S26–S32.

Frontier molecular orbitals (FMOs) study

The frontier molecular orbital energies and E_{gap} values are important variables that significantly impact the carrier transport properties, electrical properties and optical absorption of a compound[35,36]. The notion of molecular orbital theory demonstrates the inherent character of HOMO and LUMO by categorizing them as conduction and valance bands, respectively. Additionally, the transfer of charges in photovoltaic OSCs shows considerable variety as a result of the distribution patterns of HOMOs and LUMOs. Their energy difference ($\Delta E = E_{gap} = E_{LUMO} - E_{HOMO}$) is widely recognized as a fundamental metric that offers valuable insight into the photovoltaic efficiency of materials used in solar systems[37]. In this work, the central core unit and selenophene bridges lie in the same plane. However, the end-capped side chains attached to the selenophene rings are oriented at a right angle to this plane. Data obtained for the studied compounds are shown in Table 1. However, the E_{gap} of HOMO-1/LUMO + 1 and HOMO-2/LUMO + 2 is displayed in Table S8.

It is evident that the calculated E_{gap} values for the investigated compounds lie within the range of 4.433 to 4.764 eV, which is consistent with the favorable range of photovoltaic materials. The HOMO/LUMO energies of SPFR are calculated as – 7.484/– 2.558 eV. For the designed chromophores these values are investigated as follows: – 7.429/– 2.665 eV for SPF1, – 7.214/– 2.700 eV for SPF2, – 7.261/– 2.828 eV for SPF3, – 7.268/– 2.785 eV for SPF4, – 7.162/– 2.506 eV for SPF5, and – 7.035/– 2.337 eV for SPF6. Moreover, their corresponding energy gap values are as follows: 4.926 for SPFR, 4.764 eV for SPF1, 4.514 eV for SPF2, 4.433 eV for SPF3, 4.483 eV for SPF4, 4.656 eV for SPF5, and 4.698 eV for SPF6. Furthermore, the ascending order of computed E_{gap} for the model compounds under study is as follows: SPFR > SPF1 > SPF6 > SPF5 > SPF2 > SPF4 > SPF3. Among all the compounds, SPFR shows the highest E_{gap} value at 4.926 eV. The higher value might be caused by the presence of a sulphur group in its π -spacer unit. A considerable decrease in the E_{gap} value is seen in SPF1 (4.764 eV), which contains cyano groups in its end-capped acceptor moiety, i.e., 2-methylenemalononitrile, as well as thiophene is replaced by selenophene ring. This decrease could be due to the actual significant electron-

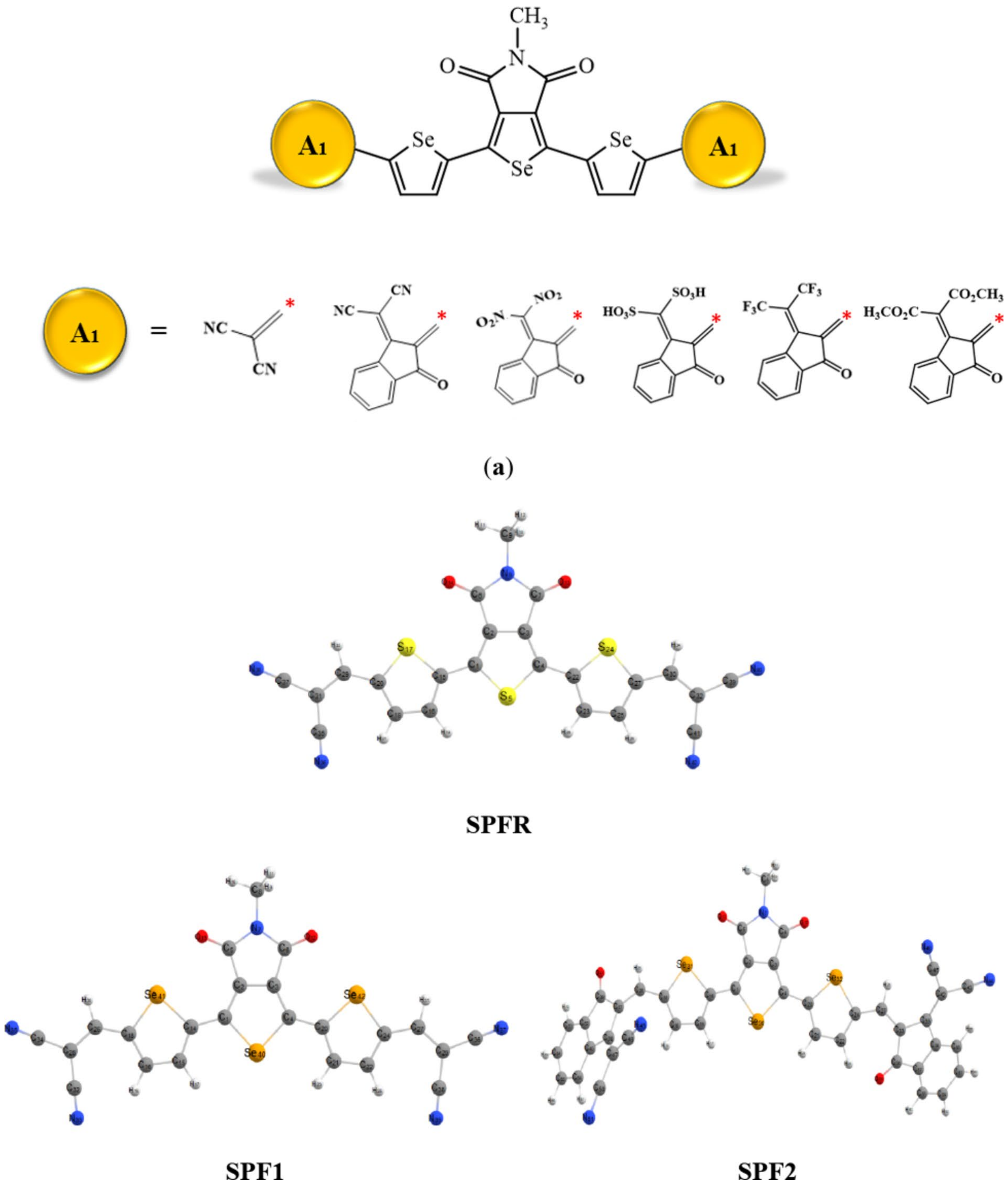

Fig. 2. (**a**) Structures of various acceptors utilized in designing of SPF1–SPF6. **(b)** Optimized geometries of SPFR, and SPF1–SPF6.

withdrawing inductive effect (-*I*) from the cyano group. A considerable decrease is found in SPF6, which might be due to the presence of ester group in the acceptor moiety. The band gap is reduced further to 4.656 eV in SPF5, which incorporates 2-methylene-3-(perfluoropropan-2-ylidene)-2,3-dihydro-1-*H*-inden-1-one as the acceptor moiety. One possible explanation for this reduced reactivity is the presence of the particularly electronegative fluoro group[38], as well as the enhancement of conjugation by the inclusion of an additional benzene ring as compared to SPF1. SPF2 (4.514 eV) shows a lower band gap than all the other molecules except SPF4. The cyano group in the acceptor units may be associated with this phenomenon, specifically 2-(2-methylene-3-oxo-2,3-dihydro-1-*H*-inden-1-ylidene) malononitrile. The cyano group exhibits an electron-withdrawing (-*I*) effect, which results in the redistribution of electron density towards the ends of the molecule[39]. This electron

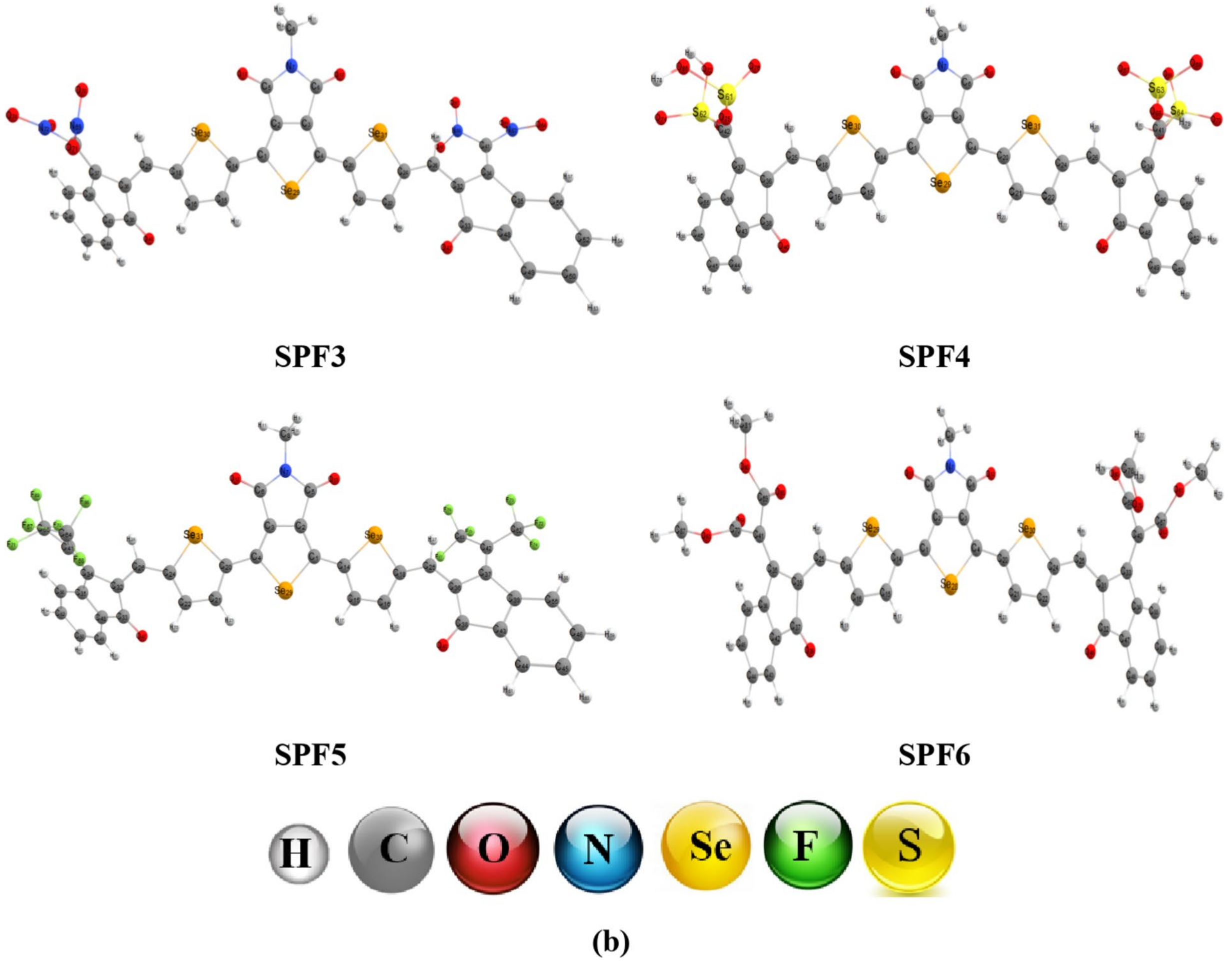

Fig. 2. (continued)

Compounds	E_{HOMO}	E_{LUMO}	ΔE
SPFR	− 7.484	− 2.558	4.926
SPF1	− 7.429	− 2.665	4.764
SPF2	− 7.214	− 2.700	4.514
SPF3	− 7.261	− 2.828	4.433
SPF4	− 7.268	− 2.785	4.483
SPF5	− 7.162	− 2.506	4.656
SPF6	− 7.035	− 2.337	4.698

Table 1. E_{HOMO}, E_{LUMO} and energy gap (E_{LUMO}-E_{HOMO}) of SPFR and studied compounds (SPF1–SPF6). E_{HOMO} = Energy of HOMO, E_{LUMO} = Energy of LUMO, $\Delta E = E_{LUMO} - E_{HOMO}$

redistribution leads to stabilization, ultimately causing a decrease in the E_{gap}. Remarkably, in SPF4, sulfonic acid is present in the peripheral acceptor (2,3-dimethylene-2,3-dihydro-1-*H*-inden-1-ylidene) methanedisulfonic acid, which is largely responsible for the least E_{gap} (4.483 eV) amid HOMO/LUMO. In the case of SPF3, the incorporation of 2-methylene-3-oxo-2,3-dihydro-1-*H*-inden-1-ylidene)methylene dinitrate as the end-capped acceptor moiety results in 4.433 eV as the band gap value. This may correspond to the pronounced electron-withdrawing effect of the highly deactivating $–NO_2$ group. Additionally, a comparative study with standard HTMs, such as spiro-OMeTAD and P3HT, demonstrated that the designed compounds exhibited reasonable band gap values, particularly for the HOMO level, making them suitable for use as HTMs in PSCs[40].

The relatively lower value compared to other chromophores indicates a significant impact of intramolecular charge transfer (ICT), leading to redshifts in the absorption spectra of the molecule. Therefore, it can be deduced that electron-withdrawing groups have a considerable impact on the energy gap, resulting in increased excitation and improved efficiency of photovoltaic materials. Figure 3 illustrates a graphical representation of the HOMO-LUMO with their associated energy gap values.

The FMOs diagrams provide insight into the spatial distribution of electron density around the HOMOs and LUMOs. Figure S2 demonstrates a significant influence of variations in the end-capped acceptor units over the distribution pattern. In case of SPFR and SPF1, the electron density in both HOMO and LUMO is seen over the entire molecule. The distribution pattern of HOMO/LUMO varies in the other derivatives (SPF2–SPF4). The distribution of HUMO occurs throughout the bridge and core unit, while the distribution of LUMO extends the whole of the structure. The charge density in the HOMOs of SPF5 and SPF6 is found on the selenophene bridge and the central core unit. On the other hand, the charge density in LUMOs resides primarily on the core unit, but a slight distribution around the whole skeleton may also be observed. Some other representations were also given in Figs. S2–S8.

Density of states

The density of states (DOS) refers to the estimation of the number of distinct states that are accessible to electrons at a given energy level[41]. To conduct a comparative analysis of their electronic properties using FMOs, we carried out density of states analysis for the designed compounds. For this purpose, we fragmented our compounds into three distinct sections namely, A_1, A_2, and π-spacer. These segments are visually represented by red, green, and blue colored line graphs, as seen in Fig. 4. In DOS pictographs, the peaks for HOMOs (valence band) depicted on left side, while the LUMOs (conduction band) exhibited at right side[42]. The charge density of HOMOs in SPFR and SPF1–SPF6 is mostly concentrated on the π-linker, with a significant presence over A_1. In case of LUMOs, it is mostly seen in A_2 motif and with a lesser presence over the π-spacer.

The findings suggested that A_1 moiety possesses a relatively large electron distribution of 32.7, 33.0, 30.8, 20.9, 30.4, 30.3, and 23.7% towards the HOMOs, while 24.4, 26.0, 17.4, 44.9, 18.6, 23.7, and 40.5% towards the LUMOs for SPFR and SPF1-SPF6, respectively. Similarly, the A_2 made respective contributions of 20.2, 19.6, 22.0, 30.9, 23.4, 22.5, and 29.1% to the HOMOs, whereas 38.3, 34.8, 54.4, 14.8, 51.3, 42.7, and 25.5% to the LUMOs, respectively. In addition, the π-spacer made successive contributions of 47.0, 47.4, 47.2, 48.2, 46.2, 47.3, and 47.1% to the HOMOs and 37.3, 39.2, 28.1, 40.2, 30.0, 33.7, and 34.0% to the LUMOs of SPFR and SPF1-SPF6. Table S25 shows the charge distribution on different fragments in the form of percentages calculated for the investigated compounds *via* DOS study.

Optical properties

The electronic excitation spectra of SPFR and SPF1–SPF6 are obtained *via* the UV-Vis analysis in solvent (chloroform) as well as in gas phases using TD-DFT calculations. The study provides significant information on the features of electronic transitions, such as the contributing configurations and the probability of charge transfer inside the molecules being studied[43]. Furthermore, this work establishes a correlation between the chemical compositions of derivatives and their efficacy as optoelectronic materials with high efficiency. Tables 2 and 3 present the optical parameters of SPFR and SPF1–SPF6, including their maximum absorption wavelength

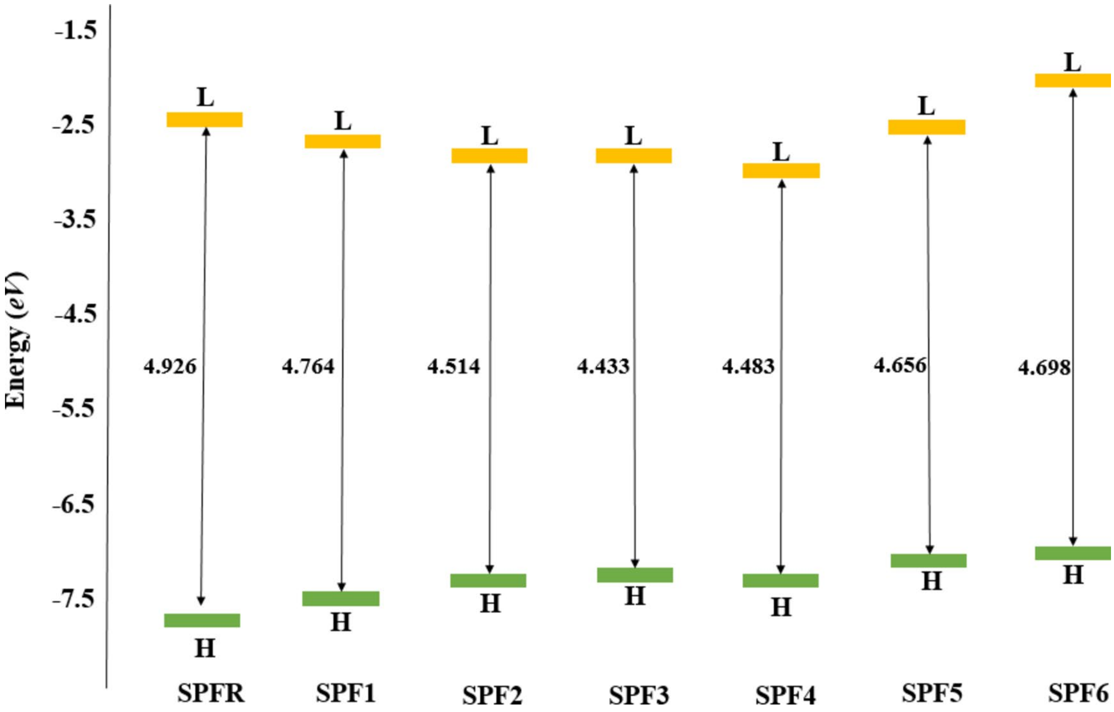

Fig. 3. Graphical representation of HOMO and LUMO energies of the SPFR and investigated compounds (SPF1–SPF6).

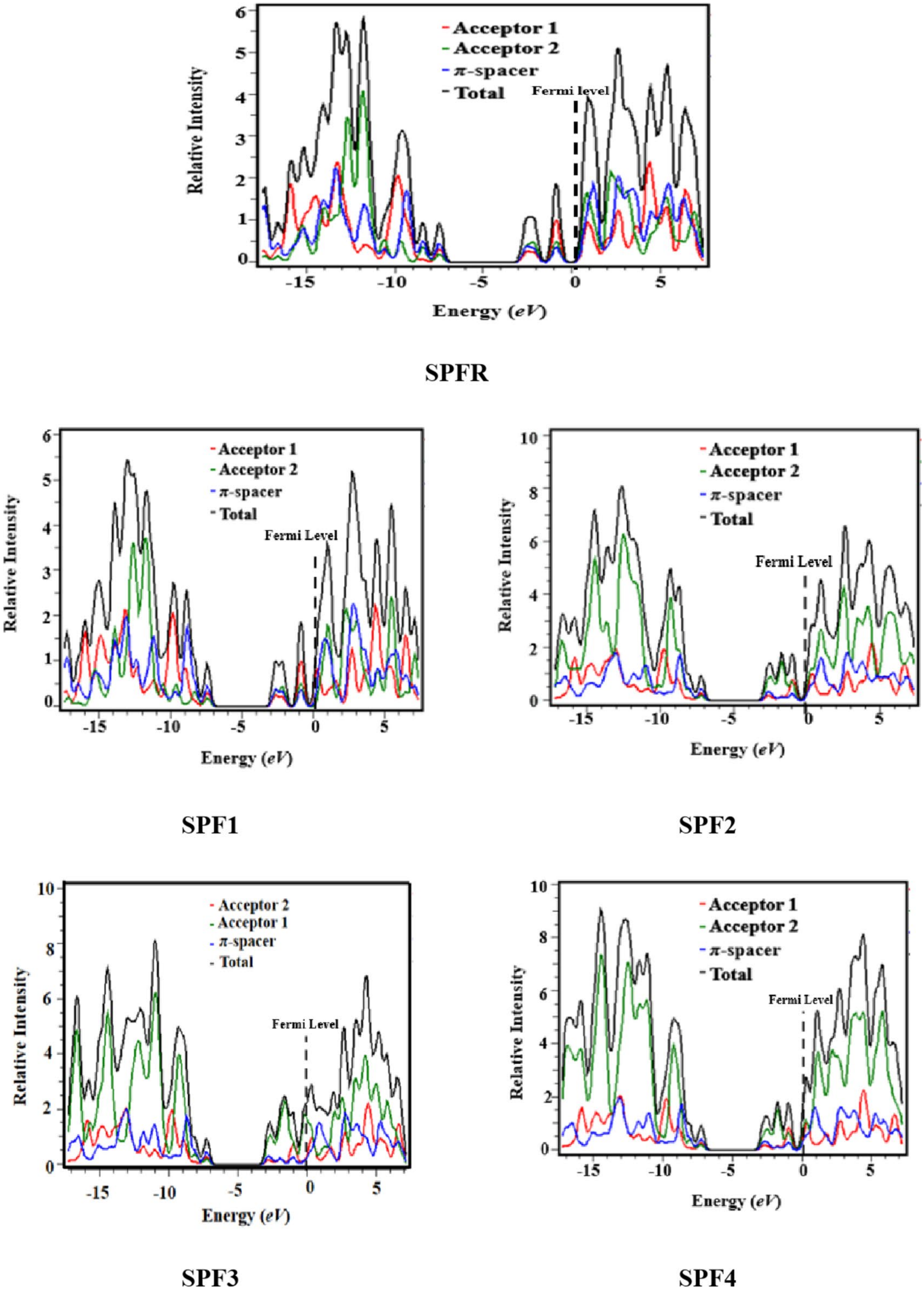

SPFR

SPF1

SPF2

SPF3

SPF4

Fig. 4. Graphical depiction of DOS for SPFR and SPF1–SPF6.

(nm), oscillation strength (f_{os}), transition energy (eV), and fundamental contributing orbitals. Moreover, Tables S9–S22 show the wavelengths other than maximum absorption wavelengths along with their corresponding transition energies and oscillation strengths. Figure 5 in the manuscript displays their UV-Vis absorption spectra in both solvent (chloroform) and gaseous phases. It is well-known from the literature that the polar medium provides an in-depth description for attaining stabilization in the π–π* state by utilizing suitable electrical levels with the intent of coupling it to the n–π* state[44]. Therefore, the interactions between dipoles and the formation of hydrogen bonds are essential for stabilizing the initial singlet energy state of a molecule. The phenomenon

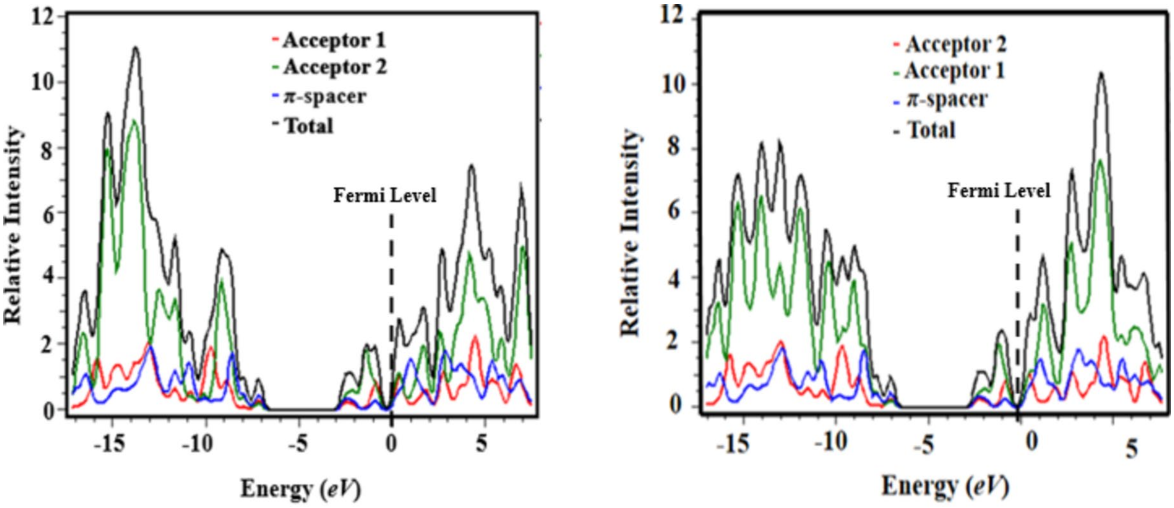

SPF5 **SPF6**

Fig. 4. (continued)

Compounds	DFT λ (nm)	E (eV)	f_{os}	LHE	MO contributions
SPFR	423.573	2.927	1.768	0.982	H→L (90%), H-1→L + 1 (7%)
SPF1	445.442	2.783	1.657	0.977	H→L (90%), H-1→L + 1 (6%)
SPF2	488.338	2.539	1.983	0.989	H→L (83%), H-1→L + 1 (11%)
SPF3	489.205	2.534	2.275	0.994	H-1→L + 1 (10%), H→L (82%)
SPF4	494.020	2.510	2.349	0.995	H→L (84%), H-1→L + 1 (11%)
SPF5	470.939	2.633	2.196	0.993	H→L (86%), H-1→L + 1 (9%)
SPF6	467.812	2.650	2.193	0.993	H→L (86%), H-1→L + 1 (9%)

Table 2. The transition energies (eV), oscillator strengths (f_{os}), maximum absorption wavelengths (λ_{max}), and transition natures of SPFR and the proposed compounds (SPF1–SPF6) in gas phase.

Compounds	DFT λ (nm)	E (eV)	f_{os}	LHE	MO contributions
SPFR	442.611	2.801	2.001	0.990	H→L (89%), H-1→L + 1 (8%)
SPF1	465.074	2.666	1.909	0.987	H→L (89%), H-1→L + 1 (7%)
SPF2	506.575	2.448	2.183	0.993	H→L (82%), H-1→L + 1 (12%)
SPF3	511.528	2.424	2.475	0.997	H-1→L + 1 (11%), H→L (79%)
SPF4	512.776	2.418	2.557	0.997	H→L (83%), H-1→L + 1 (11%)
SPF5	485.831	2.552	2.392	0.996	H→L (86%), H-1→L + 1 (10%)
SPF6	480.559	2.580	2.371	0.996	H-1→L + 1 (10%), H→L (85%)

Table 3. The transition energies (eV), oscillator strengths (f_{os}), maximum absorption wavelengths (λ_{max}), and transition natures of SPFR and the proposed compounds (SPF1–SPF6) in a solvent phase.

of bathochromic shift in the absorption wavelength is often attributed to the influence of solvent polarity. The excited state shows a much higher level of polarity compared to the ground state, leading to a more pronounced stabilization effect. The results shown in Table 3 indicate that all compounds exhibit absorbance within the UV-Visible range. Their observed maximum absorbance values (λ_{max}) indicate a more pronounced bathochromic shift (442.611–512.776 nm) in the polar solvent (chloroform) as compared to the gaseous phase, i.e., 423.573–494.020 nm (see Fig. 5). This might be attributed to the influence of solvent, as previously explained.

In gaseous phase, compound SPF4 attains the highest and the most significant bathochromic shift (λ_{max}) value at 494.020 nm and the lowest transition energy value, along with an oscillation strength of 2.349. This absorption value is well justified by the smallest E_{gap}, which is attributed to the strongly electronegative groups present in the

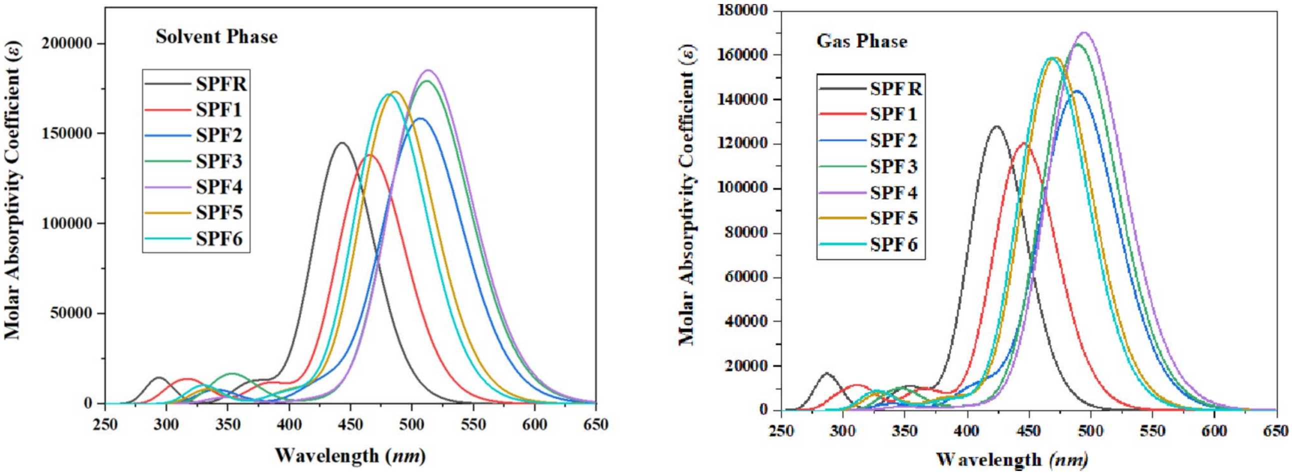

Fig. 5. UV-Vis absorption spectra of the investigated molecules in the solvent and gaseous phases.

compound. The reference compound is found with the smallest λ_{max} (423.573 nm). This absorption spectrum moves towards redshift in derivatives such as 494.020 nm in SPF4, 489.205 nm in SPF3, 488.338 nm in SPF2, 470.939 nm in SPF5, 467.812 nm in SPF6, and 445.442 nm in SPF1 as the electron-withdrawing nature of aceptors is enhanced. Their overall decreasing order of λ_{max} is as follows: SPF4 > SPF3 > SPF2 > SPF5 > SPF6 > SPF1 > SPFR (Table 2).

In chloroform, the excited state is more stabilized than the ground state, and the polarity of the ground state is lower than that of the excited state. The sequence of decreasing λ_{max} in chloroform is the same as in gaseous phase, but due to the polarity of solvent, bathochromic shift is observed in polar media: SPF4 (512.776 nm) > SPF3 (511.528 nm) > SPF2 (506.575 nm) > SPF5 (485.831 nm) > SPF6 (480.559 nm) > SPF1 (465.074 nm) > SPFR (442.611 nm). Figure 5 exhibits a graphical representation of their molar absorptivity coefficient values about their corresponding wavelengths. Furthermore, the absorption spectra of the designed compounds were compared with spiro-OMeTAD and showed correlation, highlighting their potential as alternative HTM candidates[40]. This visual representation indicates that the tailored compounds possess favorable characteristics, such as low excitation energy and high absorption wavelengths, making them candidates for utilization in the field of SCs.

Transition density matrix

TDM analysis is an alternative method for examining and assessing simulated orbitals filled by electrons. It denotes the redistribution of electron density inside a molecule, as well as the presence of electron deficiencies and surpluses following activation[45]. The TDM energy is computed with DFT model using the cam-b3lyp/6-311G(d, p) method at the first excited state. Subsequently, the data is visualized as a 2-*D* colored plot using the Multiwfn 3.7 program. The left y-axis and the bottom x-axis represent the numerical values given to non-hydrogen atoms, ranging from one to the total atom count. The exclusion of hydrogen atoms is attributable to their little impact on excitation events. The vertical axis on the right displays the electron density, while its magnitude is represented by a colour gradient ranging from blue to red. To evaluate the efficacy of the TDM, we split our designed molecules into three segments: A_1 (representing end-capped moieties), π-linker (serving as a bridge), and A_2 (representing the central core unit). Figure 6 illustrates the results of the TDM analysis for all the chromophores.

Figure 7 demonstrates the presence of electronic delocalization occurring along the diagonal of the central core (A_2) and π-linker, as well as to a lesser extent on the A_1 moiety in SPFR and SPF1–SPF6. The presence of electron density at the terminal acceptors is a crucial factor in ensuring the efficacy of our modeling technique. The study further depicts the transmission of electron density from the core towards both acceptors which is effectively facilitated *via* the selenophene bridges in all the studied chromophores. The molecule (SPF4) exhibits the most pronounced π-delocalization behavior, as seen by the presence of off-diagonal bright regions across its structure. The enhancement of PCE of OSCs has been shown *via* the use of this electron density transfer mechanism.

Exciton binding energy (E_b)

Exciton binding energy is another way of evaluating the photovoltaic properties of organic solar cells (OSCs) to explain the capacity of exciton dissociation. It is usually considered essential to assess the electrical properties, the ability to separate the excited state, and the efficiency of the work of organic solar cells[46]. Hence, determining the E_b value for both holes and electrons is a crucial parameter for understanding the interaction arising from coulombic forces. The phenomena of weakened electrostatic attraction between positively charged holes and negatively charged electrons, along with increased separation of excitons into their constituent parts, is associated with the energy transfer from the lowest energy state (S_0) to the first higher energy state (S_1)[47]. In general, lower values of E_b tend to result in increased charge dissociation, and improved PCE. Equation 1 is used

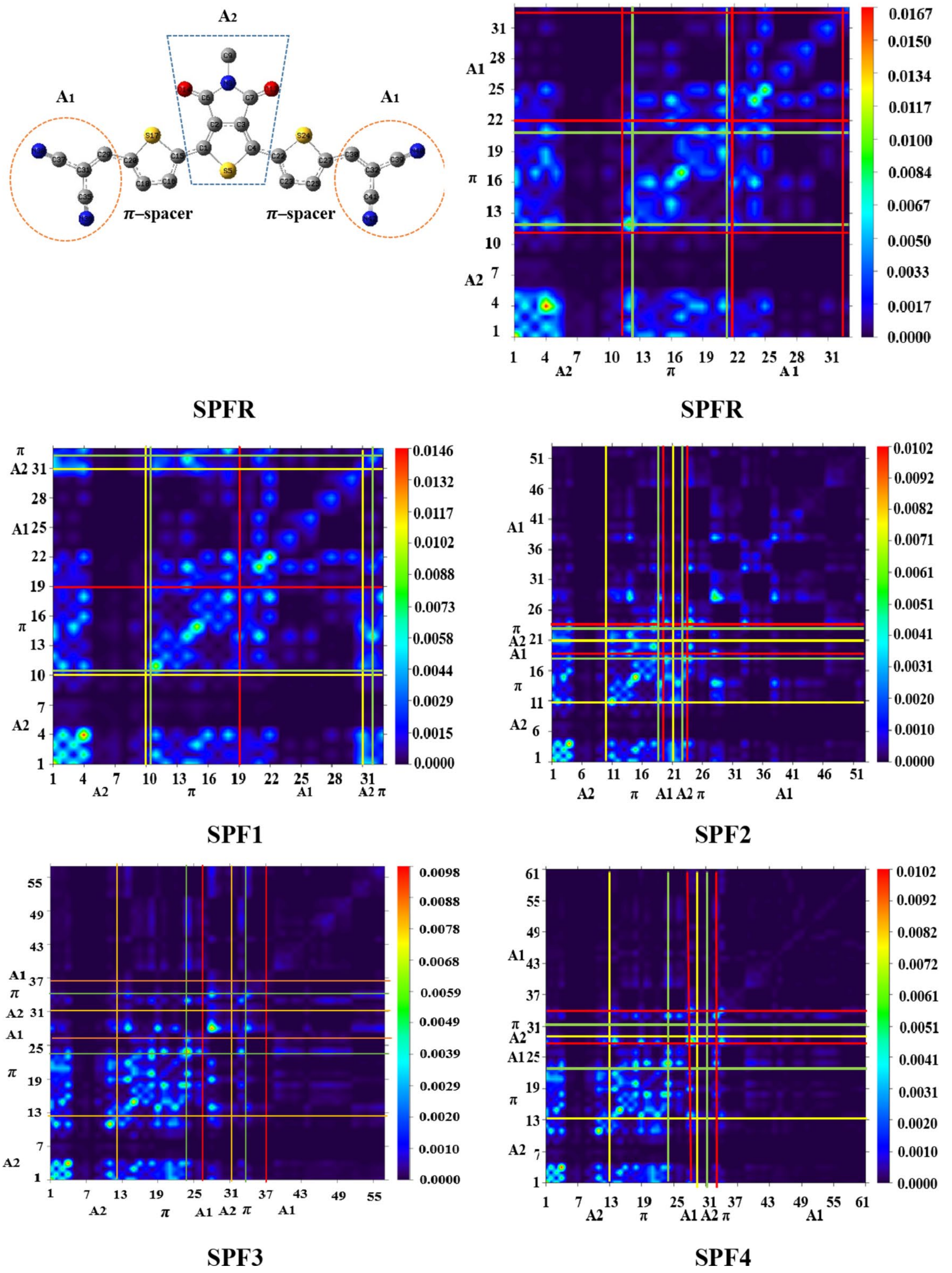

SPFR

SPFR

SPF1

SPF2

SPF3

SPF4

Fig. 6. A pictorial illustration of the hole-electron transport investigation of SPFR and SPF1–SPF6.

for the computation of the binding energy of all the compounds. Table 4 shows the results of the band gap, first excitation energy, and E_b of SPFR and SPF1–SPF6.

$$E_b = E_{H-L} - E_{opt} \tag{1}$$

Here, E_{opt} represents the minimum energy needed for the initial excitation from the ground state (S_0) to the first excited state (S_1), while E_{H-L} denotes the energy difference between HOMOs and LUMOs. The data

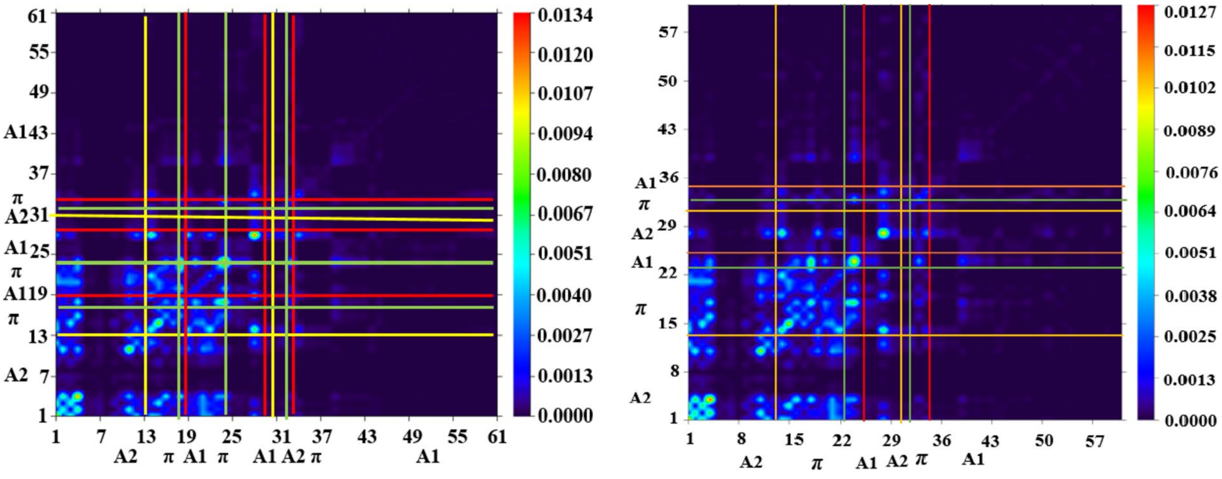

SPF5

SPF6

Fig. 6. (continued)

shown in Table 4 clearly demonstrates that designed molecules display very low levels of exciton binding energy. SPF3 has the lowest E_b value compared to the other compounds, which indicates that it has the highest abundance of charges that can easily be separated into isolated charges. Therefore, this derivative exhibits the highest level of charge segregation efficiency. Furthermore, it is worth noting that all the tailored chromophores show very high charge densities. The decreasing order of E_b in the investigated compounds is as follows: SPFR > SPF6 > SPF5 > SPF1 > SPF2 > SPF4 > SPF3. It is noteworthy to observe from this order that SPF3 demonstrates the lowest E_b as well as efficient V_{oc}, making it a suitable candidate for high-efficiency organic solar cells. Furthermore, the observed binding energy exhibits a strong correlation with the data obtained from TDM analysis.

NBO analysis

NBO analysis is the most accurate techniques for determining the bond interaction, hyperconjugation interaction, and ICT between valence and conduction band. Charge is transferred from a completely occupied donor to an acceptor using the π-spacer. The delocalization of electrons is established using the second-order perturbation technique. The results of NBOs for SPFR and SPF1–SPF6 are shown in Table S23.

It is vindicated that the top most values of π → π* transition of the R, D1,D2,D3,D4,D5 and D6 occur at 30.04, 30.46, 35.09, 35.64, 35.96, 34.16 and 33.26 kcal mol^{-1} for π(C1 – C2) → π*(C1 – C2), π(C22 – C24) → π*(C27 – C29), π(C1 – C2) → π*(C1 – C2), π(C14 – C14) → π*(C1 – C2),π(C49 – C50) → π*(C35 – C48) respectively. The bottom most values of stabilization energies are detected as 0.65, 0.59, 0.66, 0.6, 0.68, 0.63 and 0.53 kcal mol^{-1} for reference and computed compounds for π(C30 – C32) →π*(C25 – C27), π(C38 – N39) → π*(C36 – N37), and π(C61 – C65) → π*(C58 – C59), π(N72 – O74)→π*(N72 – O74),π(C3 – C4)→π*(C3 – C4),π(C37 – C42)→π*(C37 – C42),π(O65 – C69) → π*(O65 – C69) respectively. The highest values of stabilization energies for σ → σ* occur as 9.97, 9.98, 10.41, 8.84, 8.82, 8.87 and 8.9 kcal mol^{-1} of σ(C31 – C35)→σ*(C35 – N36), σ(C28 – C32)→σ*(C32 – N33), σ(C1 – C2)→σ*(C1 – C14), (C4 – Se29)→σ*(C3 – C6),(C4 – Se 29)→σ*(C3 – C6),(C1 – C14)→σ*(C1 – C2) and (C4 – Se28)→σ*(C3 – C6) for SPFR and SPF1–SPF6 respectively, and the lowest values of the same kind of transition occur as 0.93, 0.5, 0.5, 0.5, 0.5, 0.5 and 0.5 kcal mol^{-1} of σ(S17 – C20)→σ*(C18 – C20), σ(C20 – Se42)→σ*(C21 – C22), and σ(N7 – C8)→σ*(C6 – N7), σ(C15 – H17)→σ*(C4 – Se29), σ(C41-S63)→σ*(S64-O71), σ(N7-C8)→σ*(C6-N7) and σ(C2-C5)→σ*(C3-C6) respectively.

Furthermore, the highest values of LP → π* are calculated as 36.71, 25.03, 65.31, 29.35, 29.82, 28.8 and 67.8 kcal mol^{-1} of LP(S17) → π*(C15 – C16), LP(Se40) →π*(C1 – C2), and LP(Se32) → π*(C20 – C21),LP(Se30) → π*(C14 – C15), LP(Se31) → π*(C20 – C21),LP(Se29) → π*(C1 – C2) and LP(O75) → π*(O60 – C68) the highest values for LP→σ* transition observed as 32.38, 21.21, 32.17, 32.16, 32.17, 32.17 and 37.16 kcal mol^{-1} of LP(O14)→σ*(C6 – N8), LP(O12)→ σ*(C3 – C6), and LP(O13)→σ*(C5 – N7), LP(O12)→σ*(C6 – N7), LP(O12) → σ*(C6 – N7), LP(O12) → σ*(C6 – N7) and LP(O65)→σ*(C69 – O80) for the reference and designed compounds respectively. Based on NBO studies, in addition to increasing strong charge transfer, hyperconjugation play a crucial part in destabilizing the intended chromophores.

Open circuit voltage

The open circuit voltage (V_{oc}) is a potential indicator of the performance of OSCs. It represents an overall current drawn from an optical instrument[48,49]. In case of solar cells, this value is determined by measuring the current when the voltage is zero. The determination of the effect of V_{oc} encompasses several criteria, including the light source, recombination of charge carriers, temperature of OSC, external fluorescence, electrode functionality, light intensity, and multiple environmental conditions. The recombination process in solar cells is influenced by

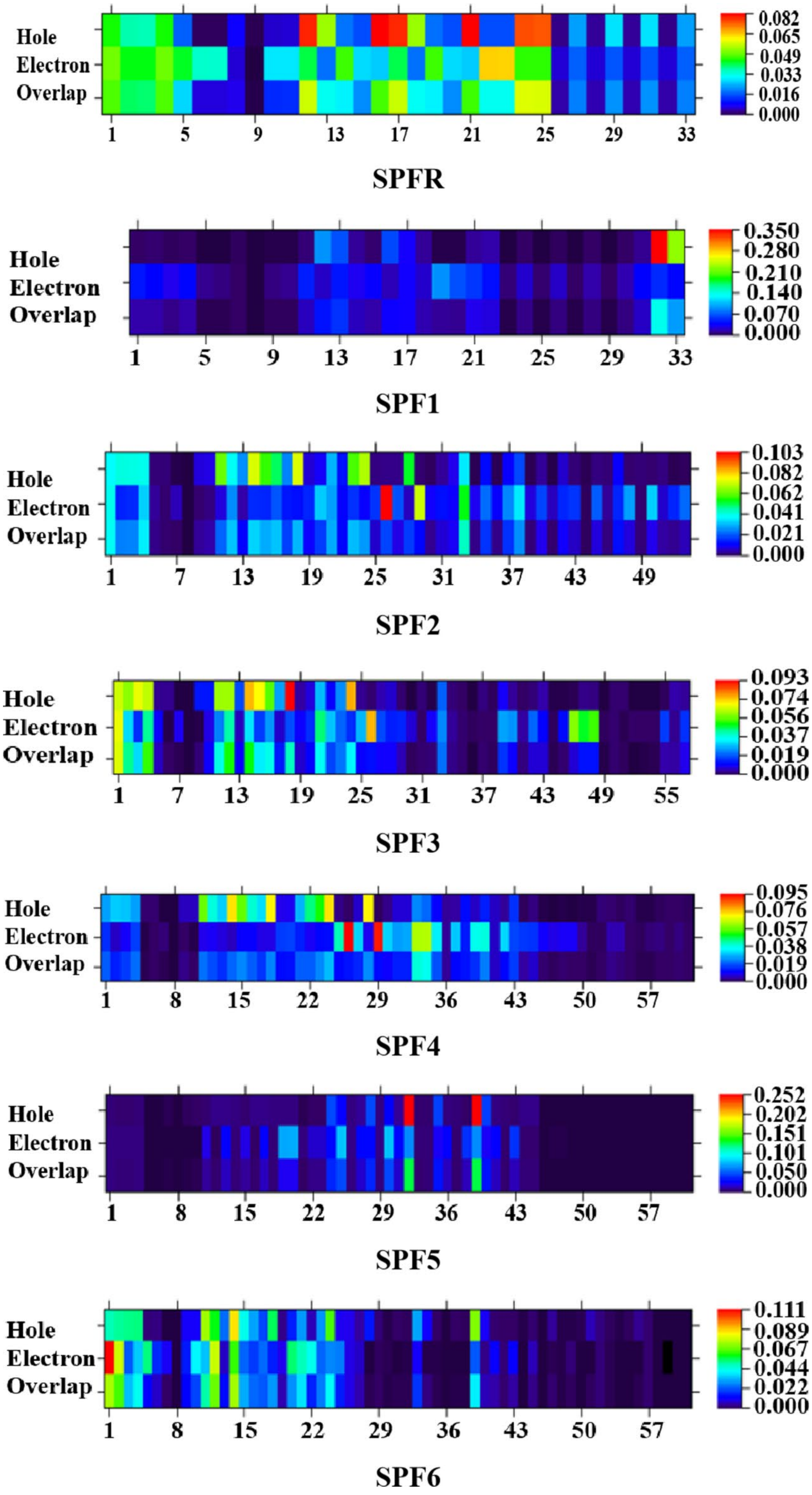

Fig. 7. TDM heat maps of the SPFR and designed compounds (SPF1–SPF6).

two significant currents: photogenerated current and saturation voltage. For accurate measurements of V_{oc}[36], it is necessary to account for certain scaling factors. Usually, the HOMO of the substance that donates electrons is aligned with LUMO of the molecule that accepts electrons. The disparity in energy levels between these orbitals is commonly referred to as the open-circuit voltage. To achieve optimal charge transfer, it is crucial for HOMO of the donor material to be situated at a lower energy level, while LUMO of the acceptor material should be positioned at a higher energy level. In this study, PTB7 (poly [4,8-bis (5- (2-ethylhexyl)thiophen-2-yl)benzo [1,2-b;4,5-b′]dithiophene-2,6-diyl-alt-(4- (2-ethylhexyl)-3-fluorothieno [3,4- b]thiophene-)-2-carboxylate-2-6-

Compounds	E_{H-L}	E_{opt}	E_b
SPFR	4.926	2.801	2.125
SPF1	4.764	2.666	2.098
SPF2	4.514	2.448	2.066
SPF3	4.433	2.424	2.009
SPF4	4.483	2.418	2.065
SPF5	4.656	2.552	2.104
SPF6	4.698	2.580	2.118

Table 4. Calculated E_b of the investigated compounds (SPF1–SPF6). Units in eV.

Compounds	λ_e (eV)[a]	Λ_h (eV)[b]
SPFR	– 0.00099065	0.00010789
SPF1	0.00055022	– 0.00009902
SPF2	0.0007155	0.00018363
SPF3	– 0.00089286	0.0003366
SPF4	0.0003827	0.0002799
SPF5	– 0.0012776	0.0002522
SPF6	0.00090782	0.00024554

Table 5. Reorganization energy (eV) of entitled compounds. [a]Reorganization energy of electron. [b]Reorganization energy of hole.

diyl) is taken as a donor polymer against SPF1–SPF6. PTB7 is a well-recognized donor material that has often been used as a donor material in previous studies. Equation 2[50] may be used to compute the open-circuit voltage in all the molecules relative to PTB7.

$$V_{oc} = \left(\left|E^{\mathrm{D}}_{\mathrm{HOMO}}\right| - \left|E^{\mathrm{A}}_{\mathrm{LUMO}}\right|\right) - 0.3 \tag{2}$$

In the above equation, $E^{\mathrm{D}}_{\mathrm{HOMO}}$ is the energy of HOMO orbital of donor and $E^{\mathrm{A}}_{\mathrm{LUMO}}$is the energy of LUMO of acceptor.

The observed values of V_{oc} for SPFR and SPF1–SPF6, with respect to the energy difference $\mathrm{HOMO}_{\mathrm{PTB7}}$–$\mathrm{LUMO}_{\mathrm{Acceptor}}$ are seen as 3.609, 3.502, 3.467, 3.339, 3.382, 3.661, and 3.830 V, respectively in Table S24. Remarkably, all the synthesized compounds have voltage values comparable to those of the reference chromophore. Among the compounds we designed, SPF6 stands out with the highest V_{oc} value recorded at 3.830 V, surpassing the energy difference observed in $\mathrm{HOMO}_{\mathrm{PTB7}}$. The findings of the V_{oc} indicate a decreasing order as SPF6 > SPF5 > SPFR > SPF1 > SPF2 > SPF4 > SPF3. Although it has already been stated early in this paper, the V_{oc} value depends mainly on the energy level of HOMO of the donor (D) and LUMO of the acceptor (A). It directly enhances the optoelectronic characteristics due to the presence of low energy LUMO of the acceptor that helps in the electron transfer from the HOMO of the D molecules. The approach promotes the effective movement of electrons from the polymer that donates them to the segment that accepts them, hence improving the researched molecular optoelectronic parameter.

Reorganizational energy

The reorganization energy of electrons and holes is another factor used to elucidate the functioning and performance of photovoltaic materials[51]. The potential OSCs mostly rely on λ, which fundamentally represents the hole and electron mobility of different materials. Usually, materials with superior charge transfer capabilities exhibit significant optoelectronic properties[52]. Reorganization energy varies under different conditions, mostly determined by the geometries of the cationic and anionic states. Electron (λ_e) mobility is associated with anionic geometry, while the hole in the material is defined by cationic geometry. λ primarily signifies the charge transfer from the donor to the acceptor unit. Reorganizational energy refers to the movements of electrons and holes inside a molecule[53]. Hole and electron reorganization energies are classified into two primary categories: (*i*) exterior and (*ii*) interior reorganization energies. inside reorganizational energy (λ_{int}) is believed to correlate with the molecule's inside environment, whereas external reorganizational energy (λ_{ext}) corresponds to the molecule's outward environment. In this context, we disregard all external stimuli and focus only on internal reorganization energy as illustrated in Table 5.

The table indicates that the λ_e of the reference compound SPFR is – 0.00099065 eV. The calculated electron mobilities of the abovementioned chromophores (SPF1-SPF6) are 0.00055022, 0.0007155, – 0.00089286, 0.0003827, – 0.0012776, and 0.00090782 eV, respectively. Among all the derivatives, SPF5 has the lowest λ_e value, indicating a superior electron transport rate between HOMO and LUMO. Likewise, SPF5 exhibits significantly enhanced electron mobilities due to its reduced λ_e value. The λ_e values of all designated chromophores decrease in the subsequent sequence SPF6 > SPF2 > SPF1 > SPF4 > SPF3 > SPFR > SPF5. The theoretically predicted λ_h of

SPFR is 0.00010789 eV. The λ_h values for SPF1-SPF6 are calculated as − 0.00009902, 0.00018363, 0.00018363, 0.0003366, 0.0002799, 0.0002522, and 0.00024554 eV, respectively. SPF1 is the superior molecule for hole transport due to its minimal λ_h value of − 0.00009902 eV. The λ_h values of all designated chromophores in decreasing order are SPF3 > SPF4 > SPF5 > SPF6 > SPF2 > SPFR > SPF1. At the same time, SPF5 is the superior candidate for electron transport, which may be used in future efficient organic solar cells.

Hole–electron analysis

The investigation of hole–electron analysis inside a molecule serves as an additional method to investigate the efficiency of solar cells[54]. This technique has proven beneficial in comprehending the movement of electronic clouds inside a compound[55]. SPFR shows a peculiar behavior as it shows charge density on many atoms. The electron intensity in SPF1 has a maximum value on C32 of the A_1 region, as shown in Fig. 6. In case of SPF2, the electron intensity is seen to be highest at C26 in the π-linkers. The observed phenomenon may be attributed to the electron-withdrawing characteristics of the cyano group and the addition of extra oxygen atoms in the A_1 region, which exert inductive influence. Moreover, in the compound SPF3, a hole appears at C18, and the electron density is maximum at C48 and C49. All the pictographs clearly depict the presence of a hole in the donor region at different atoms. Moreover, the electron intensity is shown to be greatest at certain atoms of the π-linker and gradually increases towards the acceptor moiety in all the compounds that were examined. SPF3–SPF6 exhibits electron-like behavior because the electron density within the electron band is high, whereas the density of holes is either small or non-existent. In general, the designed chromophores exhibit characteristics consistent with electron-type materials. This can be deduced from the fact that the density is maximum in the electronic band while the density of the holes is lesser in the hole band.

Non-covalent interactions (NCI) analysis

The NCI study demonstrates a significant breakthrough in molecular analysis by elucidating electron density and non-covalent interactions such hydrogen and halogen bonding, π–π stacking, and tetra bonding. A quantitative non-covalent index is created by measuring the decreased density gradient (s) and the electron density Laplacian at zero-gradient sites. This index may be visualized in two or three dimensions to precisely depict the reduced density gradient (s) and the product of electron density (ρ) with the sign of λ_2, an eigenvalue of the electron density Hessian matrix. Strong spikes in areas of low electron density and gradient magnitude are evident in the ensuing visuals, as more interactions result in a greater departure of spike amplitudes from zero. determining non-covalent interactions (NCI) requires the use of λ_2, which gives information about the nature of interactions. Negative values suggest attractive forces, whereas positive values suggest repulsive forces.

The development of NCI isosurfaces ($\rho = 0.5$) enhances the three-dimensional visualization of these interactions. Additionally, to differentiate between various types of interactions, including hydrogen bonding, van der Waals forces, and steric effects, Multiwfn 3.7 software creates a two-dimensional graphical representation called the Reduced Density Gradient (RDG). The interactions between SPFR and SPF1–SPF6 in chloroform at the CAM-B3LYP/6-311G(d, p) computational level are the subject of Fig. 8 (λ_2) ρ plots with concomitant NCI isosurfaces, which include scattered plots and RDG isosurfaces. For all of the designed derivatives, the image displays strong repulsive forces (steric effects) in red, van der Waals forces in green, and attractive forces in blue. The spectra's vertical Y-axis shows a tight density gradient, while the horizontal X-axis shows electron density, which is obtained from the product of λ_2 and ρ. With values of − 0.05 and + 0.05 atomic units (au.), respectively, the peaks at the left and right extremities indicate increased negative and positive attractions. Strong hydrogen bonds combined with less repulsive interactions lead to increased molecule stability. In the plots, the blue band (on the left) is higher than the red band (on the right), suggesting that the interactions are mostly attractive. Molecular stability is increased when favorable interactions occur more often.

The non-covalent interaction (NCI) analysis of SPFR and its derivatives (SPF1–SPF6) reveals significant insights into their molecular stability and electronic properties. The visualization of RDG plots and NCI isosurfaces highlights the dominance of attractive interactions, particularly hydrogen bonding and π–π stacking, which contribute to enhanced stability and improved charge transfer capabilities. Compounds SPF1 and SPF2 exhibit the strongest hydrogen bonding interactions, leading to superior structural integrity and promising optical properties. Conversely, SPF3 and SPF4 display moderate steric repulsion, which may slightly affect their conformational flexibility but still retain appreciable stability. SPF5 and SPF6, characterized by dominant van der Waals interactions, show relatively lower stabilization effects but maintain structural adaptability. The balance between attractive and repulsive forces across these derivatives plays a crucial role in their optoelectronic performance, making SPF1 and SPF2 the most promising candidates for applications in organic electronics and photovoltaic materials.

Conclusion

To address the limitations of fullerene acceptor molecules, it is essential to develop new fullerene-free acceptors with high power conversion efficiency. To address this issue, the end-capped acceptor structure of the NFA chromophore (SPFR) was modified by incorporating highly efficient acceptor moieties, leading to the design of A2-π-A1-π-A2 configured small molecules. Their electrical and optical characteristics have been thoroughly examined via DFT and TD-DFT methodologies. The findings demonstrated that the FMO energies and band gaps are influenced by the incorporation of various acceptor moieties. All the tailored molecules exhibited smaller band gaps and intense absorption spectra. Among these molecules, SPF3 showed the lowest band gap (4.433 eV) and the highest λ_{max} values i.e., 494.020 and 512.776 nm in gas and solvent phases, respectively. Additionally, it possessed a lower E_b value among the series of compounds (2.065 eV) which made it suitable photovoltaic material. These findings indicate that integrating electron-accepting moieties at the terminal positions is a highly effective strategy for designing efficient photovoltaic cells. Furthermore, a comparative analysis with standard

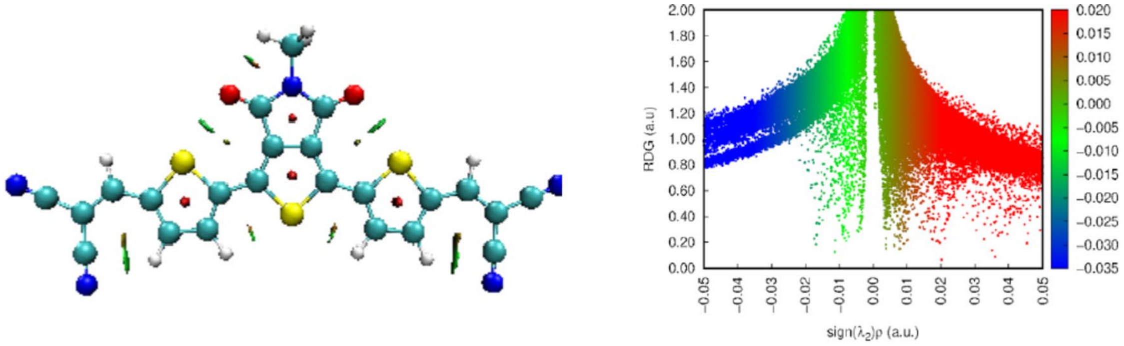

SPFR

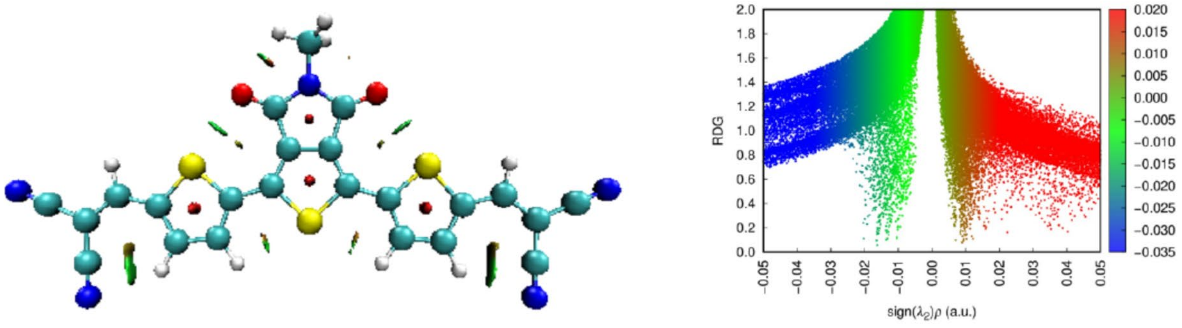

SPF1

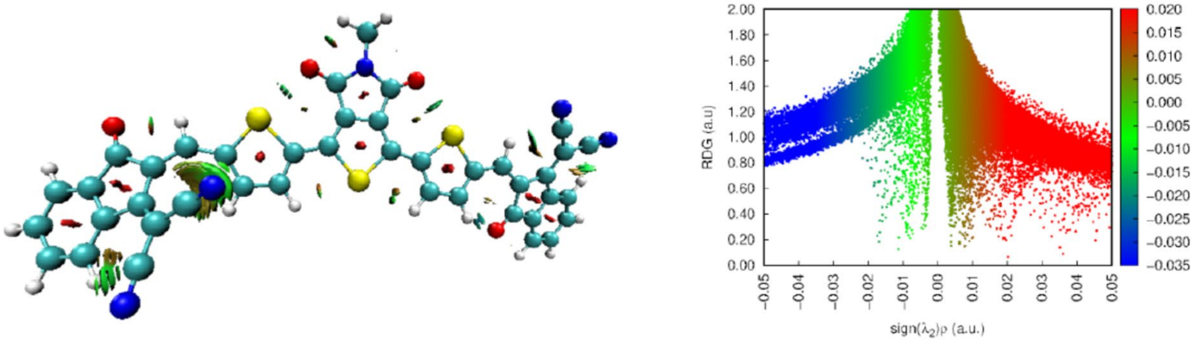

SPF2

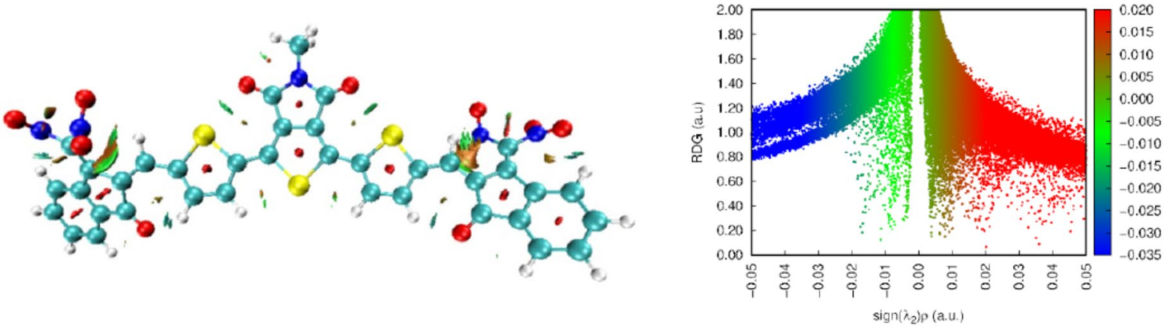

SPF3

Fig. 8. Non-covalent interactions (NCI) analysis of SPFR to SPF1–SPF6.

hole transport materials, such as spiro-OMeTAD and P3HT, demonstrated that these compounds can also serve as effective photovoltaic materials in perovskite solar cells.

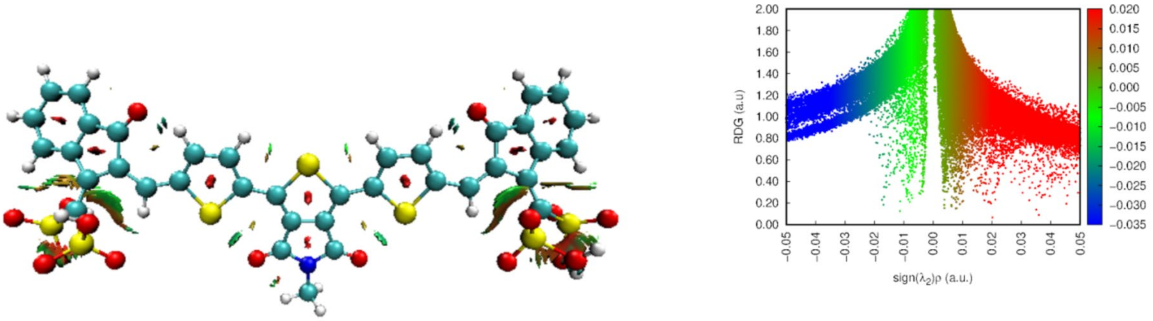

SPF4

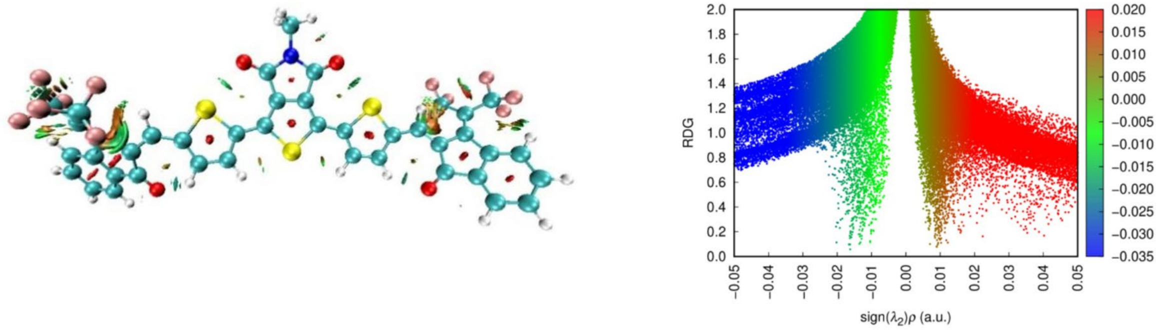

SPF5

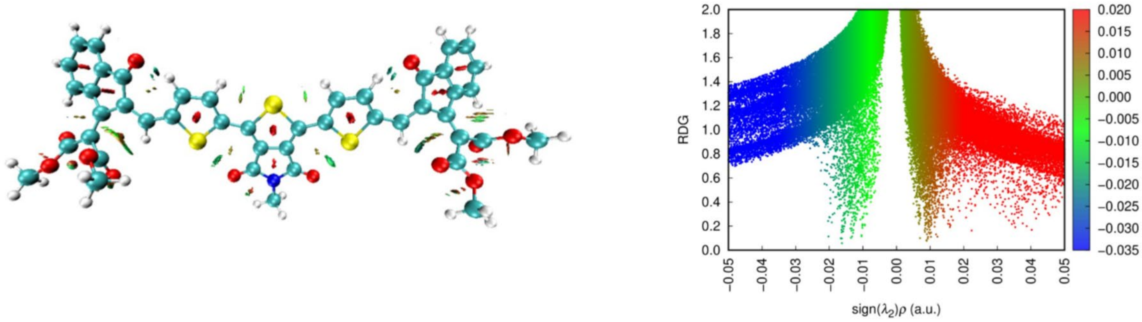

SPF6

Fig. 8. (continued)

Data availability

All data generated or analyzed during this study are included in this published article and its supplementary information files.

Received: 20 July 2024; Accepted: 21 April 2025

References

1. Li, G., Zhu, R. & Yang, Y. Polymer solar cells. *Nat. Photonics*. **6**, 153–161 (2012).
2. Cheng, P., Li, G., Zhan, X. & Yang, Y. Next-generation organic photovoltaics based on non-fullerene acceptors. *Nat. Photonics*. **12**, 131–142 (2018).
3. Yang, Y. et al. Side-chain isomerization on an n-type organic semiconductor ITIC acceptor makes 11.77% high efficiency polymer solar cells. *J. Am. Chem. Soc.* **138**, 15011–15018 (2016).
4. Zhu, L. et al. Efficient CH 3 NH 3 PbI 3 perovskite solar cells with 2TPA-n-DP hole-transporting layers. *Nano Res.* **8**, 1116–1127 (2015).
5. Chen, W. & Zhang, Q. Recent progress in non-fullerene small molecule acceptors in organic solar cells (OSCs). *J. Mater. Chem. C*. **5**, 1275–1302 (2017).
6. Arshad, M. N. et al. Enhancing the photovoltaic properties via incorporation of Selenophene units in organic chromophores with A2-π2-A1-π1-A2 configuration: A DFT-based exploration. *Polymers* **15**, 1508 (2023).
7. Bouaamlat, H., Abram, T., Bouachrine, M. & Abarkan, M. Organic dyes based on Selenophene for efficient dye-sensitized solar cell. *J. Mol. Model.* **27**, 1–10 (2021).
8. Arshad, M. N., Shafiq, I., Khalid, M. & Asiri, A. M. Exploration of the intriguing photovoltaic behavior for fused indacenodithiophene-based A–D–A conjugated systems: a DFT model study. *ACS Omega*. **7**, 11606–11617 (2022).

9. Khan, M. U. et al. First theoretical framework of Z-shaped acceptor materials with fused-chrysene core for high performance organic solar cells. *Spectrochimica Acta Mol. Biomol. Spectrosc.* **245**, 118938 (2021).
10. Aldrich, T. J. et al. Fluorination effects on indacenodithienothiophene acceptor packing and electronic structure, end-group redistribution, and solar cell photovoltaic response. *J. Am. Chem. Soc.* **141**, 3274–3287 (2019).
11. Khan, M. U. et al. In Silico modeling of new Y-Series-based near-infrared sensitive non-fullerene acceptors for efficient organic solar cells. *ACS Omega*. **5**, 24125–24137 (2020).
12. Zhang, G. et al. Nonfullerene acceptor molecules for bulk heterojunction organic solar cells. *Chem. Rev.* **118**, 3447–3507 (2018).
13. Yu, G., Gao, J., Hummelen, J. C., Wudl, F. & Heeger, A. J. Polymer photovoltaic cells: enhanced efficiencies via a network of internal donor-acceptor heterojunctions. *Science* **270**, 1789–1791 (1995).
14. Asghar, M. A. et al. Photovoltaic response promoted via intramolecular charge transfer in Triphenylpyridine core with small acceptors: A DFT/TD-DFT study. *Mater. Sci. Semiconduct. Process.* **186**, 109086 (2025).
15. Noor, T. et al. Designing thieno[3,4-*c*]pyrrole-4,6-dione core-based, A_2–D–A_1–D–A_2-type acceptor molecules for promising photovoltaic parameters in organic photovoltaic cells. *ACS Omega*. **9**, 6403–6422 (2024).
16. Tang, Y. et al. A pyrrole modified 3,4-propylenedioxythiophene conjugated polymer as hole transport layer for efficient and stable perovskite solar cells. *Small* **21**, 2408440 (2025).
17. Guo, X. et al. Thieno[3,4-*c*]pyrrole-4,6-dione-based polymer semiconductors: toward high-performance, air-stable organic thin-film transistors. *J. Am. Chem. Soc.* **133**, 13685–13697 (2011).
18. Rukhsar, J. et al. A DFT approach toward designing selenophene-based unfused small molecule acceptors by end-capped modification for improving the photovoltaic performance of organic solar cells. *J. Phys. Org. Chem.* **37**, e4587 (2024).
19. Fan, B., Lin, F., Wu, X., Zhu, Z. & Jen, A. K.-Y. Selenium-containing organic photovoltaic materials. *Acc. Chem. Res.* **54**, 3906–3916 (2021).
20. Cyr, M., Brixi, S., Ganguly, A., Lessard, B. H. & Brusso, J. L. Synthesis of Thieno [3, 4-c] pyrrole-4, 6-dione-based small molecules for application in organic thin-film transistors. *Dyes Pigm.* **210**, 110964 (2023).
21. Civalleri, B., Zicovich-Wilson, C. M., Valenzano, L. & Ugliengo, P. B3LYP augmented with an empirical dispersion term (B3LYP-D*) as applied to molecular crystals. *CrystEngComm* **10**, 405–410 (2008).
22. Adamo, C. & Barone, V. Exchange functionals with improved long-range behavior and adiabatic connection methods without adjustable parameters: the m PW and m PW1PW models. *J. Chem. Phys.* **108**, 664–675 (1998).
23. Zhao, Y. & Truhlar, D. G. The M06 suite of density functionals for main group thermochemistry, thermochemical kinetics, noncovalent interactions, excited States, and transition elements: two new functionals and systematic testing of four M06-class functionals and 12 other functionals. *Theor. Chem. Acc.* **120**, 215–241 (2008).
24. Yanai, T., Tew, D. P. & Handy, N. C. A new hybrid exchange–correlation functional using the Coulomb-attenuating method (CAM-B3LYP). *Chem. Phys. Lett.* **393**, 51–57 (2004).
25. Andersson, M. P. & Uvdal, P. New scale factors for harmonic vibrational frequencies using the B3LYP density functional method with the triple-ζ basis set 6-311 + G (d, p). *J. Phys. Chem. A*. **109**, 2937–2941 (2005).
26. Frisch, M. J. et al. *Gaussian 09* 150–166 (Gaussian, 2009).
27. Dennington, R. D., Keith, T. A. & Millam, J. M. *GaussView 5.0* (Gaussian, 2008).
28. O'boyle, N. M., Tenderholt, A. L., Langner, K. M. & Cclib A library for package-independent computational chemistry algorithms. *J. Comput. Chem.* **29**, 839–845 (2008).
29. Lu, T., Chen, F. & Multiwfn A multifunctional wavefunction analyzer. *J. Comput. Chem.* **33**, 580–592 (2012).
30. Hanwell, M. D. et al. Avogadro: an advanced semantic chemical editor, visualization, and analysis platform. *J. Cheminform.* **4**, 1–17 (2012).
31. Zhurko, G. A. & Zhurko, D. A. *ChemCraft, Version 1.6*. http://www.chemcraftprog.com (2009).
32. Wang, J. et al. Effect of nitro-substituted ending groups on the photovoltaic properties of nonfullerene acceptors. *ACS Appl. Mater. Interfaces*. **12**, 41861–41868 (2020).
33. Yao, C. et al. Elucidating the key role of the cyano (‒C≡N) group to construct environmentally friendly fused-ring electron acceptors. *J. Phys. Chem. C*. **124**, 23059–23068 (2020).
34. Shafiq, I. et al. Use of benzothiophene ring to improve the photovoltaic efficacy of cyanopyridinone-based organic chromophores: a DFT study. *RSC Adv.* **14**, 12841–12852 (2024).
35. Zhang, Y. et al. Tuning the molecular geometry and packing mode of non-fullerene acceptors by altering the Bridge atoms towards efficient organic solar cells. *Mater. Chem. Front.* **4**, 2462–2471 (2020).
36. Hussain, R. et al. Enhancement in photovoltaic properties of N, N-diethylaniline based donor materials by bridging core modifications for efficient solar cells. *ChemistrySelect* **5**, 5022–5034 (2020).
37. Srnec, M. & Solomon, E. I. Frontier molecular orbital contributions to chlorination versus hydroxylation selectivity in the non-heme iron halogenase SyrB2. *J. Am. Chem. Soc.* **139**, 2396–2407 (2017).
38. Zhang, B., Shi, G., Yang, Z., Zhang, F. & Pan, S. Fluorooxoborates: beryllium-free deep-ultraviolet nonlinear optical materials without layered growth. *Angew. Chem. Int. Ed.* **56**, 3916–3919 (2017).
39. Yao, C. et al. Elucidating the key role of the cyano (- C\equiv N) group to construct environmentally friendly fused-ring electron acceptors. *J. Phys. Chem. C*. **124**, 23059–23068 (2020).
40. Li, S., Cao, Y. L., Li, W. H. & Bo, Z. S. A brief review of hole transporting materials commonly used in perovskite solar cells. *Rare Met.* **40**, 2712–2729 (2021).
41. Khan, M. U. et al. First theoretical probe for efficient enhancement of nonlinear optical properties of Quinacridone based compounds through various modifications. *Chem. Phys. Lett.* **715**, 222–230 (2019).
42. Khan, M. U. et al. Novel W-shaped oxygen heterocycle-fused fluorene-based non-fullerene acceptors: first theoretical framework for designing environment-friendly organic solar cells. *Energy Fuels*. **35**, 12436–12450 (2021).
43. Ans, M., Iqbal, J., Ayub, K., Ali, E. & Eliasson, B. Spirobifluorene based small molecules as an alternative to traditional fullerene acceptors for organic solar cells. *Mater. Sci. Semiconduct. Process.* **94**, 97–106 (2019).
44. Khalid, M., Lodhi, H. M., Khan, M. U. & Imran, M. Structural parameter-modulated nonlinear optical amplitude of acceptor–π–D–π–donor-configured pyrene derivatives: A DFT approach. *RSC Adv.* **11**, 14237–14250 (2021).
45. Köse, M. E. Evaluation of acceptor strength in thiophene coupled donor–acceptor chromophores for optimal design of organic photovoltaic materials. *J. Phys. Chem. A*. **116**, 12503–12509 (2012).
46. Köse, M. E. et al. Theoretical studies on conjugated phenyl-cored thiophene dendrimers for photovoltaic applications. *J. Am. Chem. Soc.* **129**, 14257–14270 (2007).
47. Dkhissi, A. Excitons in organic semiconductors. *Synth. Met.* **161**, 1441–1443 (2011).
48. Hussain, S. et al. Designing novel Zn-decorated inorganic B12P12 nanoclusters with promising electronic properties: a step forward toward efficient CO2 sensing materials. *ACS Omega*. **5**, 15547–15556 (2020).
49. Scharber, M. C. et al. Design rules for donors in bulk-heterojunction solar cells—Towards 10% energy-conversion efficiency. *Adv. Mater.* **18**, 789–794 (2006).
50. Scharber, M. C. et al. Design rules for donors in bulk-heterojunction solar cells—towards 10% energy-conversion efficiency. *Adv. Mater.* **18**, 789–794 (2006).
51. Khalid, M. et al. First theoretical framework for highly efficient photovoltaic parameters by structural modification with benzothiophene-incorporated acceptors in Dithiophene based chromophores. *Sci. Rep.* **12**, 20148 (2022).

52. Qiao, L. et al. Novel alternative for controlling enzymatic Browning: catalase and its application in fresh-cut potatoes. *J. Food Sci.* **86**, 3529–3539 (2021).
53. Khan, M. U. et al. Molecular designing of high-performance 3D star-shaped electron acceptors containing a Truxene core for nonfullerene organic solar cells. *J. Phys. Org. Chem.* **34**, e4119 (2021).
54. Hassan, T. et al. Development of non-fused acceptor materials with 3D-Interpenetrated structure for stable and efficient organic solar cells. *Mater. Sci. Semiconduct. Process.* **151**, 107010 (2022).
55. Ans, M. et al. Designing three-dimensional (3D) non-fullerene small molecule acceptors with efficient photovoltaic parameters. *ChemistrySelect* **3**, 12797–12804 (2018).

Acknowledgements

Dr. Muhammad Khalid gratefully acknowledges the financial support of HEC Pakistan (project no. 20-14703/NRPU/R&D/HEC/2021). A.A.C.B. (grant 2015/01491-3) is highly thankful to Fundação de Amparo à Pesquisa do Estado de São Paulo for the cooperation and financial assistance. A.A.C.B. (grant 312550/2020-0) also thanks to the Brazilian National Research Council (CNPq) for financial support and fellowship. The authors also thank the Researchers Supporting Project number (RSPD2025R645), King Saud University, Riyadh, Saudi Arabia.

Author contributions

Muhammad Khalid: Supervision; Investigation; Resources; software; project administration; Methodology; Fatima Tayyab: Formal analysis; Investigation; Writing - original draft; Visualization; Muhammad Adeel: Conceptualization; Resources; software; Formal analysis; Validation; Nayab Tahir: Formal analysis; Investigation; Writing - original draft; Visualization; Ataualpa A. C. Braga: Conceptualization; Resources; software; Formal analysis; Validation; Khalid Abdullah Alrashidi: Data Curation; Writing - review & editing; Formal analysis, Funding acquisition.

Declarations

Competing interests

The authors declare no competing interests.

Additional information

Supplementary Information The online version contains supplementary material available at https://doi.org/10.1038/s41598-025-99585-6.

Correspondence and requests for materials should be addressed to M.K.

Reprints and permissions information is available at www.nature.com/reprints.